



OPEN Prognostic impact of tertiary lymphoid structures and cancer-associated fibroblasts in hepatocellular carcinoma with portal vein tumor thrombus

Lingbo Hu^{1,2,3,10}, Cong Chen^{1,4,10}, Yanhong Xiao^{5,6,7}, Zhenghang Li¹, Ning Jiang^{5,6}, Chengyou Du¹, Guirong Lv⁸✉, Jun Tang^{1,7}✉ & Bo Zeng⁹✉

The significance of tertiary lymphoid structures (TLS) in hepatocellular carcinoma (HCC) with portal vein tumor thrombus (PVTT) remains ambiguous. This study evaluates the prognostic impact of intra-tumoral TLS (iTLS) and peri-tumoral TLS (pTLS) and explores the interplay between TLS and cancer-associated fibroblasts (CAF) in patients undergoing curative hepatic resection. A retrospective analysis of 83 HCC patients with PVTT assessed the prognostic value of TLS. Transcriptomic data were mined to identify TLS- and CAF-related genes, and a seven-gene prognostic model was constructed using LASSO and Cox regression analyses. Immune microenvironment, mutation characteristics, and response to immunotherapy were analyzed between risk groups. iTLS+ and high pTLS density were independently associated with improved overall survival (OS), but not recurrence-free survival (RFS) or early recurrence. A novel risk model comprising *KLF2*, *HBEGF*, *KLRB1*, *PGF*, *JAM2*, *CHORDC1*, and *YTHDF2* stratified patients into high- and low-risk groups, with the high-risk group demonstrating poorer OS and diminished immunotherapy responsiveness. Low-risk patients exhibited higher immune infiltration (e.g., B cells, T cells) and stronger antitumor activity, whereas high-risk tumors showed active proliferation and immune evasion. iTLS and pTLS are independent predictors of favorable OS in HCC patients with PVTT. The TLS/CAF-based risk model offers robust prognostic utility and highlights distinct biological and immune features between patient subgroups. These findings provide a foundation for personalized prognostic assessment and therapeutic decision-making in advanced HCC.

Keywords Hepatocellular carcinoma, Portal vein tumor thrombus, Tertiary lymphoid structures, Cancer-associated fibroblast, Prognostic model

Abbreviations

TLS	Tertiary Lymphoid Structures
PVTT	Portal Vein Tumor Thrombus
HCC	Hepatocellular Carcinoma
iTLS	Intra-tumor TLS

¹Department of Hepatobiliary Surgery, The First affiliated Hospital of Chongqing Medical University, Chongqing, China. ²Department of Hepatopancreatobiliary Surgery, Taizhou Hospital of Zhejiang Province Affiliated to Wenzhou Medical University, Taizhou, Zhejiang, China. ³Department of Hepatopancreatobiliary Surgery, Enze Hospital, Taizhou Enze Medical Center (Group), Taizhou, Zhejiang, China. ⁴Department of Hepatobiliary Surgery, Bishan Hospital of Chongqing Medical University, Bishan Hospital of Chongqing, Chongqing 402760, China. ⁵Department of Pathology, School of Basic Medical Sciences, Chongqing Medical University, Chongqing, China. ⁶Molecular Medicine Diagnostic and Testing Center, Chongqing Medical University, Chongqing, China. ⁷Key Laboratory of Molecular Oncology and Epigenetics, The First Affiliated Hospital of Chongqing Medical University, Chongqing, China. ⁸Bijie Hospital of Zhejiang Provincial People's Hospital, Bijie, China. ⁹The Affiliated Yongchuan Hospital of Chongqing Medical University, Chongqing, China. ¹⁰Lingbo Hu and Cong Chen contributed equally to this work and should be considered co-first authors. ✉email: 13885729710@163.com; tjcherish023@163.com; zengbo@hospital.cqmu.edu.cn

pTLS	Peritumor TLS
HBV	Hepatitis B Virus
RFS	Recurrence-free Survival
OS	Overall Survival
CI	Confidence Interval
HR	Hazard Ratio
BCLC	Barcelona Clinic Liver Cancer
AASLD	American Association for the Study of Liver Diseases
TACE	Transarterial Chemoembolization
TKIs	Tyrosine Kinase Inhibitors
ICIs	Immune Checkpoint Inhibitors
CT	Computed Tomography
MRI	Magnetic Resonance Imaging
AFP	Alpha-fetoprotein
H&E	Hematoxylin and Eosin
ALB	Albumin
PT	Prothrombin Time
APTT	Activated Partial Thromboplastin Time
ALT	Alanine Aminotransferase
AST	Aspartate Aminotransferase
TB	Total Bilirubin
HCV	Hepatitis C Virus
AFP	Alpha-fetoprotein
MVI	Microscopic Vascular Invasion
CAF	Cancer-associated Fibroblast
FFPE	Formalin-fixed Paraffin-embedded
DEG	Differentially Expressed Genes
ROC	Receiver Operator Characteristic
AUC	Area Under the Curve
FC	Fold Change
GO	Gene Ontology (GO)
KEGG	Kyoto Encyclopedia of Genes and Genomes
GSEA	Gene set enrichment analysis

Hepatocellular carcinoma (HCC), the most prevalent form of liver cancer, demonstrates the third-highest incidence and sixth-highest mortality rates globally¹. Typically, HCC is diagnosed in its intermediate to advanced stages, with fewer than 30% of cases being operable in the early stages^{2,3}. According to the Barcelona Clinic Liver Cancer (BCLC) staging system, HCC with portal vein tumor thrombus (PVTT) is classified as BCLC stage C. The guidelines from the European Association for the Study of the Liver (EASL) and the American Association for the Study of Liver Diseases (AASLD) recommend transarterial chemoembolization (TACE) or systemic therapy for patients with BCLC stage B or C^{4,5}. However, a meta-analysis has shown that patients with BCLC stage B or C who undergo surgical intervention have superior survival outcomes compared to those treated with TACE or sorafenib⁶. The advent and clinical implementation of tyrosine kinase inhibitors (TKIs) and immune checkpoint inhibitors (ICIs) have significantly improved the survival outcomes of patients with unresectable intermediate to advanced liver cancer following systemic treatment. This has enabled the downstaging of certain advanced HCC cases, making them suitable for resection. Although patients with HCC and PVTT have increased opportunities for liver resection, it is important to note that high-risk factors for recurrence, such as tumor size exceeding 5 cm, multiple tumors, satellite nodules, or microvascular invasion, particularly PVTT, significantly elevate the likelihood of recurrence^{7–13}. The immune contexture and spatial organization of immune cells have emerged as critical determinants in influencing tumor invasion, metastasis, and ultimately the prognosis of patients with malignancies^{14–16}.

Tertiary lymphoid structures (TLS) are acquired ectopic lymphoid formations that develop in non-lymphoid tissues in response to chronic inflammation and neoplastic conditions. These structures are categorized based on the presence of follicles and germinal centers, reflecting a multistage maturation process: early TLS (lymphoid aggregates), primary TLS (follicles without germinal centers), and secondary TLS (follicles with germinal centers)¹⁷. The presence of TLS has been correlated with favorable prognostic outcomes in various malignancies, including breast¹⁸, lung¹⁹, colorectal²⁰, and pancreatic cancers²¹. However, the prognostic significance of TLS in HCC remains controversial. While Finkin et al. analyzed clinical data, validated findings in murine models, and investigated potential mechanisms at the protein and gene levels, concluding that TLS presence indicates a poor prognosis in human HCC, subsequent studies have contradicted these findings, demonstrating a positive association between TLS and improved prognosis in HCC patients^{22–24}. Notably, previous studies predominantly included patients with BCLC stage 0–A, with only about 20% comprising patients with BCLC stage B–C, leaving the role of TLS in the prognosis of HCC patients with PVTT unexplored. Therefore, our study focuses on surgically resected HCC patients with PVTT to elucidate the correlation between TLS and prognosis in this specific cohort. We used public databases to further explore which TLS-related genes are involved in the relevant molecular mechanisms.

Cancer-associated fibroblasts (CAF), as critical components of the tumor microenvironment, also play a significant role in HCC progression and prognosis. CAFs are known to facilitate tumor growth, immune evasion, and metastasis by secreting cytokines, chemokines, and extracellular matrix components. Interestingly, CAFs

seem to interact with TLS within the tumor microenvironment, potentially influencing immune responses and patient outcomes. While CAFs are generally associated with poor prognosis due to their immunosuppressive roles, they may also contribute to the formation of TLS by promoting chemokine production, such as CXCL13, which is involved in lymphocyte recruitment. This dual role of CAFs highlights the complexity of their relationship with TLS and underscores the need for further investigation into the CAF-TLS interaction in HCC.

Methods

Clinical analysis

Patients and samples

The study was conducted in accordance with the Declaration of Helsinki 1964 and its later amendments. This investigation received authorization from the Ethics Committee of the First Affiliated Hospital of Chongqing Medical University, with informed consent procured preoperatively for the utilization of surgical specimens and associated clinical data. The cohort of HCC patients presenting with PVTT underwent hepatectomy for HCC at the First Affiliated Hospital of Chongqing Medical University between January 2017 and August 2023. The inclusion criteria were as follows: (1) Histopathological confirmation of hepatocellular carcinoma; (2) Detection of PVTT via dynamic contrast-enhanced computed tomography (CT) or magnetic resonance imaging (MRI); (3) Patients undergoing radical hepatic resection. Exclusion criteria encompassed: (1) Patients with recurrent HCC; (2) Patients with combined hepatocellular-cholangiocarcinoma. Recorded clinical and biological parameters included age, sex, HBV infection, HCV infection, hepatic function, Child-Pugh classification, liver cirrhosis, BCLC staging, preoperative alpha-fetoprotein (AFP) serum levels, tumor dimension, microvascular invasion, tumor multiplicity, tumor differentiation, and PVTT classification (vp1 to vp4). Follow-up involved hepatic imaging via CT scan or MRI.

The primary clinical endpoints are overall survival (OS), recurrence-free survival (RFS), and early recurrence. OS was calculated from the date of hepatectomy to the date of death or, for surviving patients, to the date of the last follow-up. RFS was delineated as the interval from surgical resection to recurrence or progression, mortality from any cause, or the last follow-up. Early recurrence was characterized as recurrence manifesting within two years post-hepatectomy.

Pathological examination

Pathological sections encompassing both neoplastic and peritumoral tissues were utilized for histopathological assessment. The peritumoral tissue was harvested from a margin of 5 mm adjacent to the tumor boundary. Dual sections were prepared for hematoxylin and eosin (H&E) staining and were independently evaluated by two seasoned pathologists. All sections were digitized using a 40x objective lens, followed by analysis with the Motic DSAssistant software to ascertain the presence of intra-tumoral TLS (iTLS). Motic Image Plus software facilitated the quantification of the peritumoral tissue area and the enumeration of pTLS. The density of pTLS was calculated as the number of pTLS per unit area of peritumoral tissue (per mm²). For result interpretation, sections devoid of TLS were categorized as iTLS⁻, while those containing TLS were classified as iTLS⁺. The median density of pTLS was employed as a threshold to bifurcate pTLS into two cohorts. Specimens exceeding the median were designated as pTLS⁺, and those below the median as pTLS⁻. In HE-stained pathological sections, the fibrotic thickness within and surrounding the tumor was additionally measured, and the maximum value recorded.

Immunohistochemistry

We performed immunohistochemical tests on sections with mature TLS to observe some immune cells in mature TLS. Formalin-fixed, paraffin-embedded tumor blocks were used for preparation of 4-mm thick serial sections. Immunohistochemistry and quantitation of tumor-infiltrating immune cells were performed as previously described²⁴. Slides were stained for CD3, CD4, CD8, and PDL1.

Statistical analysis

Categorical variables underwent comparison utilizing either the chi-square test or Fisher's exact test. Continuous variables were subjected to comparison employing the t-test, Mann-Whitney U test, or Kruskal-Wallis rank test. Survival curves were constructed utilizing the Kaplan-Meier method and juxtaposed utilizing the log-rank test. Univariate Cox proportional hazards regression analysis was employed to identify prognostic risk factors. Factors exhibiting a p-value < 0.05 were included in the Multivariate Cox proportional hazards regression analysis. A significance level of $p < 0.05$ was adopted. All statistical analyses were conducted using SPSS software (version 26.0, SPSS Inc., Chicago, IL, USA). Survival curves were generated using R software (version 4.4.0).

Bioinformatics analysis

We created a flowchart to illustrate the complete workflow of the bioinformatics analysis (Fig. 1).

Source of data analysis

The RNA expression data of hepatocellular carcinoma (TCGA-LIHC), SNP data and clinical information were downloaded from the TCGA database (<https://portal.gdc.cancer.gov/>) as the training set. Only primary HCC samples with survival time longer than 0 days in TCGA-LIHC were included (365 samples). ICGC-LIRI was downloaded from the ICGC database (<https://dcc.icgc.org/>). GSE14520 was downloaded from the GEO database (<https://www.ncbi.nlm.nih.gov/gds>). CLCA cohort was downloaded from the Genome Sequence Archive in BIG Data Center, Beijing Institute of Genomics (BIG), Chinese Academy of Sciences (<https://ngdc.cncb.ac.cn/bioproject/browse/PRJCA002666>)²⁵. The latter three datasets were validation sets. In the follow-up study, 39 TL S-related genes were from the existing reports²⁶. CAF-related genes were from CAFrgDB²⁷.

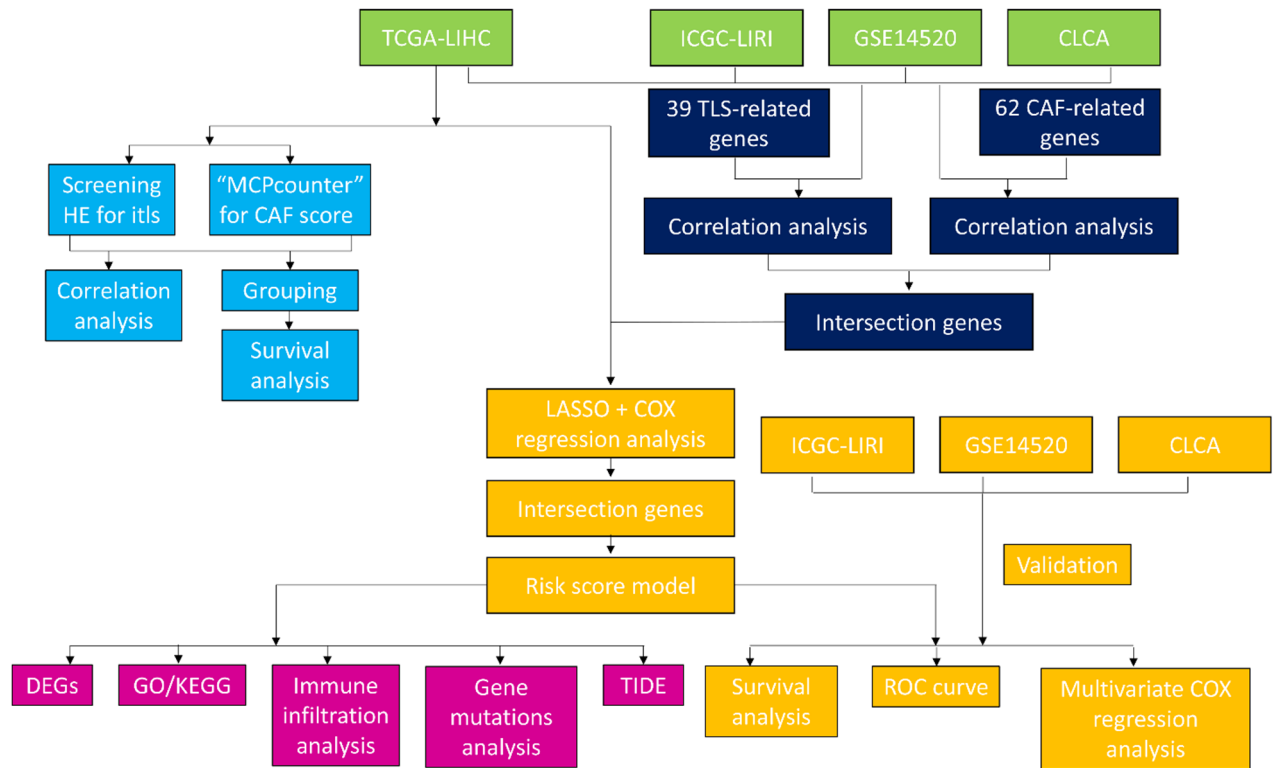


Fig. 1. Schematic workflow of the comprehensive bioinformatics analysis pipeline.

Evaluation of *i*TLS in pathological sections

We evaluated the density of lymphocyte infiltration by retrieving HE pathologically stained sections of the corresponding TCGA samples from the Cancer Digital Slide Archive (CDSA). Frozen sections and formalin-fixed paraffin-embedded (FFPE) tissue sections were used. The definition of *i*TLS+/- was mentioned above.

Analysis of the impact of *i*TLS and CAF score on the overall survival of HCC

CAF score of every sample in TCGA-LIHC was calculated using MCPcount package. The difference in CAF score between *i*TLS+ and *i*TLS- group was calculated using Kruskal test. The samples were divided into CAF high and CAF low groups, bounded by the median CAF score. According to *i*TLS+/- and CAF high/low, the samples were divided into four groups, namely *i*TLS+CAF high, *i*TLS+CAF low, *i*TLS-CAF high, and *i*TLS-CAF low. The Kaplan-Meier Curve was used to explore whether the patients in the four groups had different OS.

Construction of prognostic model based on TLS-related and CAF-related genes

Genes with Pearson correlation coefficient >0.5 and $p < 0.05$ for TLS-related genes were extracted from the four datasets. Similarly, genes with Pearson correlation coefficient >0.5 and $p < 0.05$ for CAF-related genes were extracted from the four datasets. The genes obtained after the intersection of these genes were used as candidate genes for subsequent analysis. Univariate Cox regression analysis of candidate genes was performed using the R package 'survival' to screen genes significantly associated with prognosis ($P < 0.05$). In order to prevent over-fitting of the model, R package 'glmnet' was used to perform Lasso-Cox regression analysis on the genes screened by univariate Cox regression analysis to obtain candidate feature genes. R package 'survival' was used to further screen the candidate characteristic genes by two-way stepwise regression method, and a multivariate Cox regression model was constructed for the genes significantly associated with prognosis, and the forest plot was drawn by R package 'survminer'.

Prognostic model validation

According to the median value of the model risk score, the samples were divided into high and low risk groups, and the R package 'pheatmap' was used to draw the model characteristic gene heat map, as well as the risk score distribution map and the survival status distribution map. Kaplan-Meier survival analysis was performed on the high and low risk groups using the R package 'survival', and the receiver operator characteristic (ROC) curve was drawn using the R package 'timeROC' to obtain the area under the curve (AUC) values of the 1-, 3-, and 5-year overall survival (OS). The above steps are verified in ICGC-LIRI, GSE14520, and CLCA.

Analysis of gene expression differences between high risk and low risk groups

We performed differential expression analysis using the R package "DESeq2" according to the risk grouping (high risk or low risk). First, samples with zero expression were excluded. Differential expression analysis was

performed to explore differences between the two groups with the $|\log_2$ fold change (FC)| >3 and adjusted p -value < 0.01.

Biological functional analysis

We used R package “clusterProfiler” for gene ontology (GO) biological processes, GO cellular composition, GO molecular function, and Kyoto Encyclopedia of Genes and Genomes (KEGG) enrichment analyses^{28–30}. Univariate cox regression was used to screen out genes associated with OS for GO and KEGG analysis. Additionally, gene set enrichment analysis (GSEA) was performed using the Canonical pathways sets and ontology gene sets to clarify the signaling pathways in the locations of the differential genes.

Analysis of immune microenvironment in high and low risk groups

The R package ‘estimate’ was used to evaluate the tumor microenvironment of each sample in high and low risk, and the immune score, matrix score, ESTIMATE score and tumor purity of each sample were calculated. R package ‘GSVA’ was used for ssGSEA analysis to visualize the differential enrichment of immune-related cells and functions in high and low risk groups. The ‘CIBERSORT’ package was used to analyze the differences of 22 immune cell infiltration levels in the high-and low-risk groups.

Analysis of mutation characteristics in high and low risk groups

R package ‘mafools’ was used to visualize the mutation sites of high-frequency mutant genes in high-and low risk groups, and to explore the co-mutation and mutual exclusion between them.

Prediction of response to immunotherapy by risk score

TIDE algorithm was used to predict the response to immunotherapy. The prediction of response to immunotherapy was compared between high-risk score group and low-risk score group by Wilcoxon test.

Prognostic risk model independence verification

In each dataset, univariate Cox regression analysis was performed using the R package ‘survival’ in combination with clinical features and risk scores, and forest plots were drawn using the R basic package. Multivariate Cox regression analysis was performed using the R package ‘survival’, and the forest plot was drawn using the R basic package to determine whether the risk score could be used as an independent prognostic factor.

Immunohistochemistry of target gene

We downloaded the immunohistochemistry data of the target gene from the Human Protein Atlas (HPA) database to compare the differences in target gene expression between normal liver tissue and HCC tumor tissue.

Results

Clinical results

Clinicopathological characteristics of patients

A total of 83 patients diagnosed with surgically treated HCC were included in the study. The demographic and clinicopathological characteristics are outlined in Table 1. In this cohort, 28 patients (33.7%) tested positive for iTLS+, while 55 were negative (iTLS-). Notably, the iTLS+ group exhibited a higher proportion of patients with AFP levels > 400 ng/ml and thicker fibrotic encasement around the tumor (Fig. 2A). Furthermore, the peri-tumoral fibrotic thickness was notably thicker in the pTLS- group (Fig. 2B). Among the 28 cases positive for iTLS, lymphoid follicles with germinal centers were observed in 2 cases (7.1%), lymphoid follicles without germinal centers were observed in 2 cases (7.1%), and lymphoid aggregates were identified in 24 cases (85.7%) (Fig. 3). Immunohistochemical assessments revealed elevated expressions of CD3, CD4, CD8, and PDL1 within mature TLSs. A median of 1.38 pTLS per square millimeter was observed, with a range of 0.16–6.22. Patients with a pTLS density exceeding 1.38 were classified as pTLS+, while those below were categorized as pTLS-. At a median follow-up duration of 16.1 months (range: 0.2–83.7 months), 23 deaths (27.7%) were recorded, and tumor recurrence was experienced by 45 patients (54.2%).

Association between TLS and survival

The outcomes of both univariate and multivariate analyses are presented in Fig. 4 and Table S1. Survival curves are displayed in Fig. 5. In the univariate analysis, both iTLS+ and pTLS+ were associated with improved OS (hazard ratio (HR): 0.349, 95% confidence interval (CI): 0.128–0.948, $p = 0.039$, HR: 0.365, 95% CI: 0.153–0.869, $p = 0.023$). This prognostic significance of iTLS+ and pTLS+ remained significant even after adjusting for other factors in the multivariate analysis (HR: 0.287, 95% CI: 0.103–0.799, $p = 0.042$, HR: 0.397, 95% CI: 0.160–0.985, $p = 0.025$). The presence of HBV infection was correlated with poorer RFS (HR: 3.288, 95% CI: 1.175–9.202, $p = 0.023$). Furthermore, although not reaching statistical significance, pTLS+ exhibited a potential association with improved RFS in the univariate analysis (HR: 0.558, 95% CI: 0.311–1.003, $p = 0.051$). Only the presence of PVTT with vascular invasion grades 3 and 4 was linked to heightened early recurrence in the univariate analysis (HR: 1.819, 95% CI: 1.159–2.854, $p = 0.009$).

Bioinformatics results

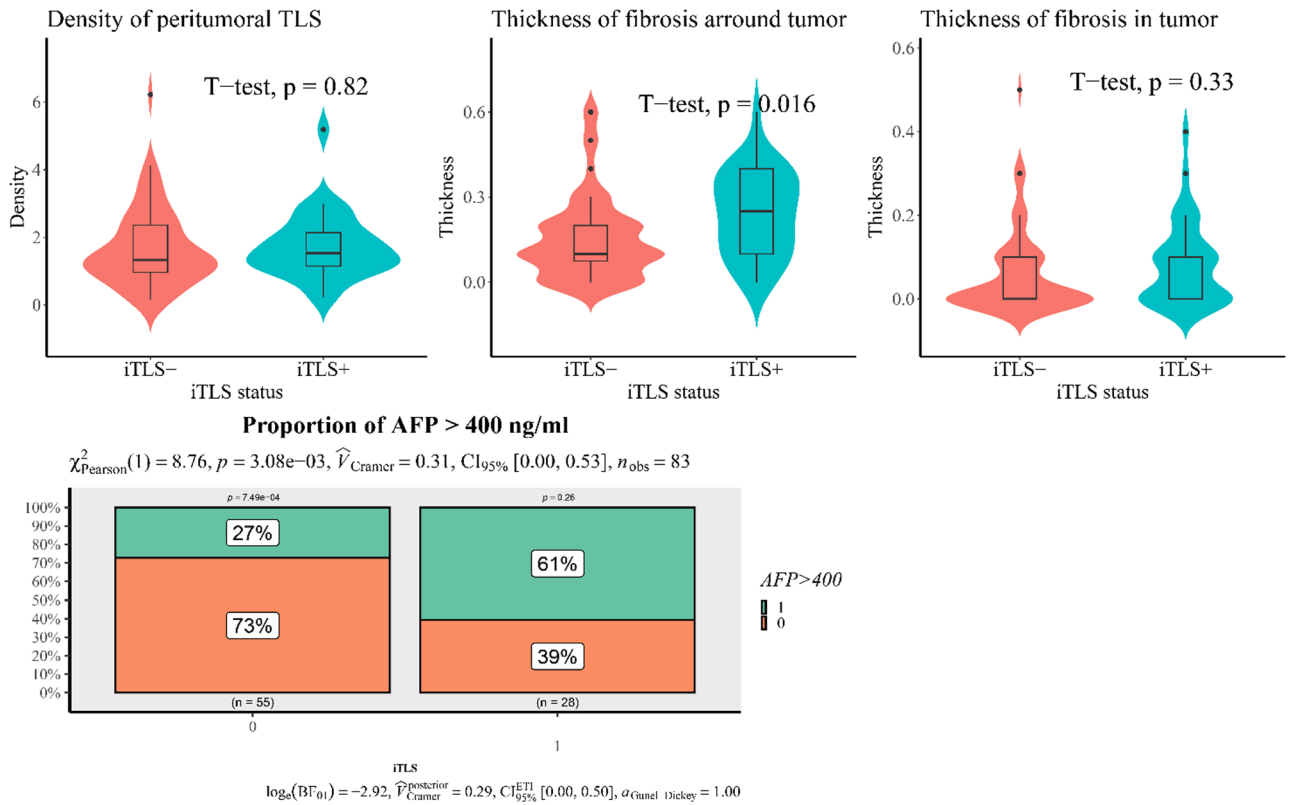
The relationship between iTLS and CAF with OS in TCGA cohort

The clinical characteristics of publication databases were shown in Table S2–5. The median value of CAF score was significantly higher in iTLS+ group than iTLS- group (Fig. 6A). Patients with high CAF score or low CAF score had similar OS (Fig. 6B). Patients with iTLS+ achieved better OS (Fig. 6C). According to iTLS+/- and CAF

Variables	iTLS + (n=28)	iTLS - (n=55)	p value	pTLS + (n=42)	pTLS - (n=41)	p value
Age (year)	54.54 ± 9.26	53.29 ± 11.84	0.629	53.36 ± 8.66	54.07 ± 13.07	0.769
Gender			0.428			0.261
Male	22	47		33	36	
Female	6	8		9	5	
Child Pugh score			0.879			0.743
5	22	44		34	32	
6	6	11		8	9	
Alb (g/L)	40.46 ± 4.57	39.98 ± 5.45	0.689	39.40 ± 4.88	40.90 ± 5.35	0.187
PT (s)	13.41 ± 0.96	13.64 ± 0.68	0.216	13.63 ± 0.82	13.49 ± 0.76	0.436
APTT (s)	37.71 ± 5.49	37.83 ± 4.93	0.921	38.19 ± 5.29	37.39 ± 4.92	0.48
ALT (U/L)	48.14 ± 28.25	44.62 ± 27.89	0.592	46.76 ± 27.38	44.83 ± 28.71	0.754
AST (U/L)	54.93 ± 41.38	48.47 ± 33.91	0.449	48.76 ± 36.30	52.59 ± 37.00	0.636
TB (μmol/L)	13.79 ± 7.33	15.80 ± 12.92	0.45	14.13 ± 14.17	16.13 ± 7.46	0.424
Cause of hepatitis						
HBV	25	43	0.214	33	35	0.421
HCV	0	1	0.361	1	0	1
Cirrhosis			0.21			0.189
Positive	16	39		25	30	
Negative	12	16		17	11	
AFP (ng/ml)			0.003			0.591
≤ 400	11	40		27	24	
>400	17	15		15	17	
Tumor size (cm)	7.15 ± 3.66	7.80 ± 3.75	0.449	7.00 ± 3.78	8.18 ± 3.58	0.147
Tumor number			0.659			0.212
Solitary	18	38		31	25	
Multiple	10	17		11	16	
MVI			0.073			0.567
Positive	20	28		23	25	
Negative	8	27		19	16	
Tumor differentiation			0.922			0.931
Poor	17	34		26	25	
moderate or well	11	21		16	16	
Type of portal vein tumor thrombus			0.421			0.519
vp1	2	3		4	1	
vp2	8	24		15	17	
vp3	15	26		20	21	
vp4	2	2		3	2	
Fibrotic thickness around the tumor (mm)	0.24 ± 0.15	0.16 ± 0.15	0.014	0.14 ± 0.14	0.23 ± 0.15	0.005
Fibrotic thickness in the tumor (mm)	0.09 ± 0.10	0.06 ± 0.10	0.329	0.04 ± 0.06	0.10 ± 0.13	0.003
Treatment after recurrence	14	24	0.7511	22	23	0.9049
Hepatectomy	4	8		8	4	
RFA	1	3		2	2	
TACE	5	15		9	11	
HAIC	2	1		1	2	
Radiotherapy	2	2		1	3	
Best supportive care		1			1	
Pulmonary lobectomy		1		1		

Table 1. Characteristics of patients and tumors. *Abbreviations* iTLS, Intratumoral Tertiary Lymphoid Structures; pTLS, Peritumoral Tertiary Lymphoid Structures; Alb, Albumin; PT, Prothrombin Time; APTT, Activated Partial Thromboplastin Time; ALT, Alanine Aminotransferase; AST, Aspartate Aminotransferase; TB, Total Bilirubin; HBV, Hepatitis B Virus; HCV, Hepatitis C Virus; AFP, Alpha-Fetoprotein; MVI, Microvascular Invasion; RFA, Radiofrequency Ablation; TACE, Transarterial Chemoembolization; HAIC, Hepatic Arterial Infusion Chemotherapy.

A. Factors related to iTLS



B. Factors related to pTLS



Fig. 2. The factors related to iTLS and pTLS in the Whole cohort.

high/low, patients were divided into four groups, and the OS of patients in different groups were different (Fig. 6D).

Construction and validation of HCC prognostic model based on TLS-related and CAF-related genes

In this study, a total of 1020 genes were obtained from the intersection of the genes obtained by differential analysis and the results of co-expression analysis (Figure S1 and Table S6). Univariate Cox regression analysis combined with Lasso-Cox regression analysis of these genes resulted in 13 candidate characteristic genes (Fig. 7A and B). Multivariate Cox regression analysis was performed on 13 candidate characteristic genes, and finally 7 characteristic genes related to TLS and prognosis were obtained (Fig. 7C and D). A prognostic model was constructed for the characteristic genes according to the following formula: Risk Score = $-0.5065 \times KLF2 + 0.3211 \times HBEGF - 0.4313 \times KLRB1 + 0.6668 \times PGF - 0.4453 \times JAM2 + 0.4837 \times CHORDC1 + 0.5908 \times YTHDF2$.

The characteristic gene expression heat map of the model showed that HBEGF, PGF, CHORDC1, YTHDF2 genes were highly expressed in the high-risk group, while KLF2, KLRB1, JAM2, were lowly expressed in the high-risk group (Figure S2). The Risk Score distribution map shows that Risk Score is higher in the high-risk group. At the same time, the survival status distribution map shows that the number of patient deaths gradually increases with the increase of Risk Score (Figure S2). The results of survival analysis showed that the overall survival rate of patients in the high-risk group was lower and showed a worse prognosis level (Fig. 7E-H). ROC analysis showed that the AUC values of the TCGA-LIHC set for predicting the 1-, 3-, and 5-year prognostic

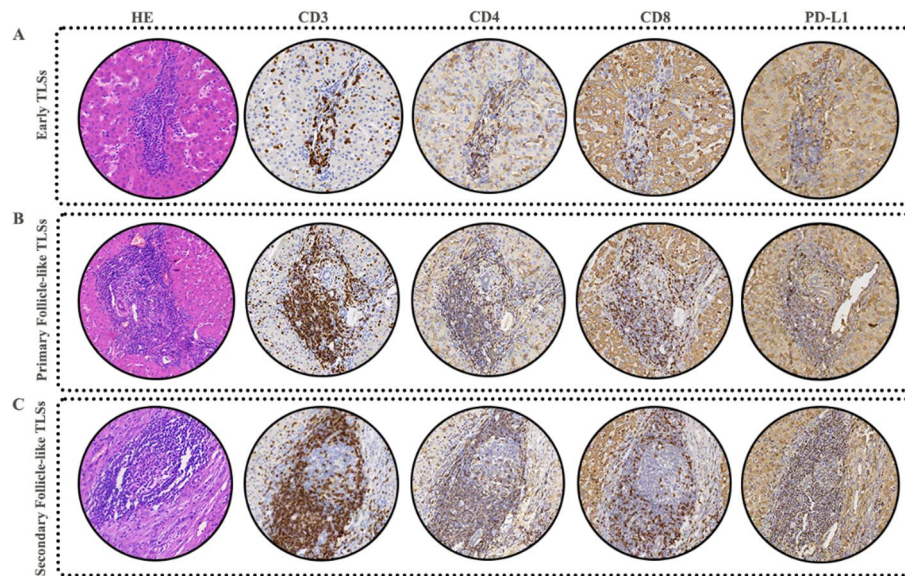


Fig. 3. Different maturity of tertiary lymphoid structures (TLSs) identified through hematoxylin and eosin (H&E) staining and the immunohistochemistry of immune cell in corresponding maturity tertiary lymphoid structures. (A) Early TLSs; (B) Primary follicle-like TLSs; (C) Secondary follicle-like TLSs.

survival rates of patients were 0.677, 0.731, and 0.687, respectively (Fig. 7I). The AUC values of the ICGC set for predicting the 1-, 3-, and 5-year prognostic survival rates of patients were 0.573, 0.624, and 0.607, respectively (Fig. 7J). The AUC values of the GSE14520 set for predicting the 1-, 3-, and 5-year prognostic survival rates of patients were 0.546, 0.562, and 0.594, respectively (Fig. 7K). The AUC values of the CLCA set for predicting the 1-, 2-, and 3-year prognostic survival rates of patients were 0.604, 0.650, and 0.614, respectively (Fig. 7L). The above results indicate that the 7 gene model has a good predictive effect on the prognosis of HCC patients.

Differential genes between low-risk and high-risk groups

The results of the differential expression analysis showed that of the 1273 differential genes, most (1196 genes) were upregulated, whereas the expression of the other 77 showed varying degrees of downregulation (Table S7). The volcano maps of DEGs between high and low risk groups and the top 50 DEGs are shown in Figure S3. Among them, 557 genes were associated with OS (Table S8).

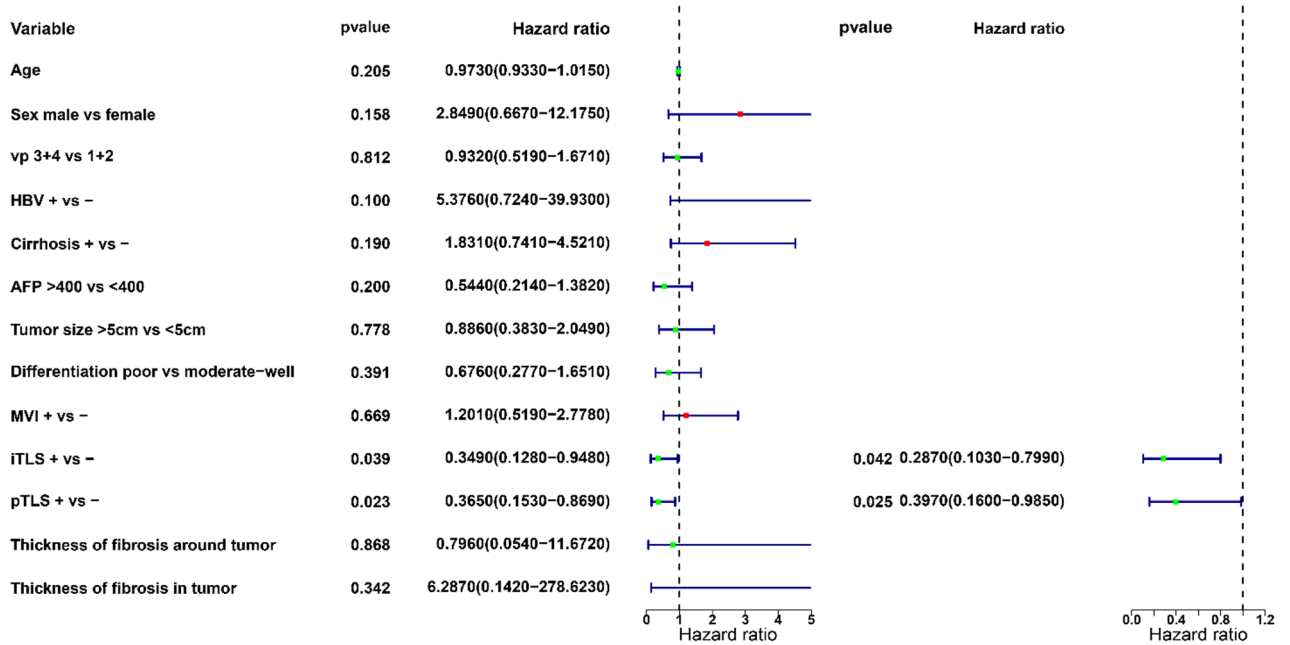
Differentially expressed genes (DEGs) are associated with multiple biological functions

We discovered enrichment in biological process (BP), namely, organelle fission, nuclear division, and chromosome segregation; cellular component (CC), namely, spindle, chromosomal region, and chromosome, centromeric region; molecular function (MF), namely, microtubule binding, DNA-binding transcription activator activity, and motor activity (Fig. 8A). The KEGG analysis showed high enrichment in cell cycle, oocyte meiosis, and motor protein (Fig. 8B). We used gene sets enrichment analysis (GSEA) to investigate the differentially active pathways between the high-risk and low-risk groups. We discovered immune response, cytokines and antigen-antibody reaction pathways were significantly enriched in low-risk group, such as adaptive immune response, immune response signaling pathway, lymphocyte mediated immunity, immunoglobulin complex, allograft pathway, inflammatory response, antigen processing, cytokine-receptor interaction (Fig. 8C, D). While high-risk group showed enrichment in metabolic related pathways and cell growth and differentiation related pathways, such as steroid hormone synthesis, retinol metabolism, drug metabolism cytochrome P450, and epidermal cell differentiation (Fig. 8E, F).

Analysis of immune components in high and low risk groups

To explore the relationship between the model risks core and the regulation of immune infiltration microenvironment, this study evaluated the differences in immune cell scores and immune component scores between high and low risk groups. We found that the levels of these immune indicators in the high-risk group were similar to those in the low-risk group through ssGSEA analysis (Fig. 9A). The results from ESTIMATE showed that Immune Score in the high-risk group were significantly higher than those in the low-risk group (Fig. 9B). CIBERSORT analysis showed that B cells, T cells, and DC cells had significantly higher infiltration levels in the low-risk group (Fig. 9C and Table S9). These results indicate the differences in immune characteristics between high-and low-risk groups, and the lower level of immune component infiltration in the high-risk group also suggests worse anti-tumor immune activity.

Univariate and multivariate cox regression analysis for overall survival



Univariate cox regression analysis for overall survival

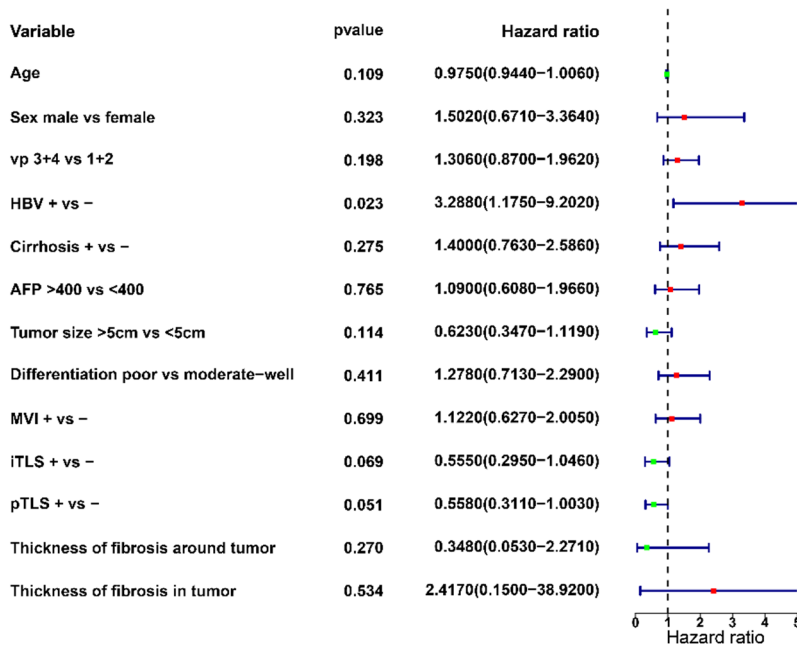


Fig. 4. The results of univariate and multivariate cox regression analysis for overall survival and recurrence-free survival of patients. Abbreviations: HR, hazard ratio; iTLS, intratumor tertiary lymphoid structure; pTLS, peritumor tertiary lymphoid structure; HBV, hepatitis virus B; AFP, alpha-fetoprotein; MVI, microscopic vascular invasion.

Differences in mutation characteristics between high and low risk groups

The top 20 genes of mutation frequency in all samples in TCGA dataset were shown in Figure S4. The top 20 genes of mutation frequency in the high and low risk groups were analyzed. There were differences in the top 20 mutation genes between the high and low risk groups, and the mutation frequency was also different. It is worth noting that the frequency of TP53 mutations in the high-risk group was significantly higher than that in the low-risk group (Table S10, Fig. 10A and B). The gene co-mutation and mutually exclusive mutation map showed that the proportion of co-mutation and mutually exclusive mutation in the low-risk group was larger than that in the high-risk group (Fig. 10C and F). These results indicate the heterogeneity of gene mutation patterns between high and low risk groups, which may be one of the factors leading to differential prognosis between samples.

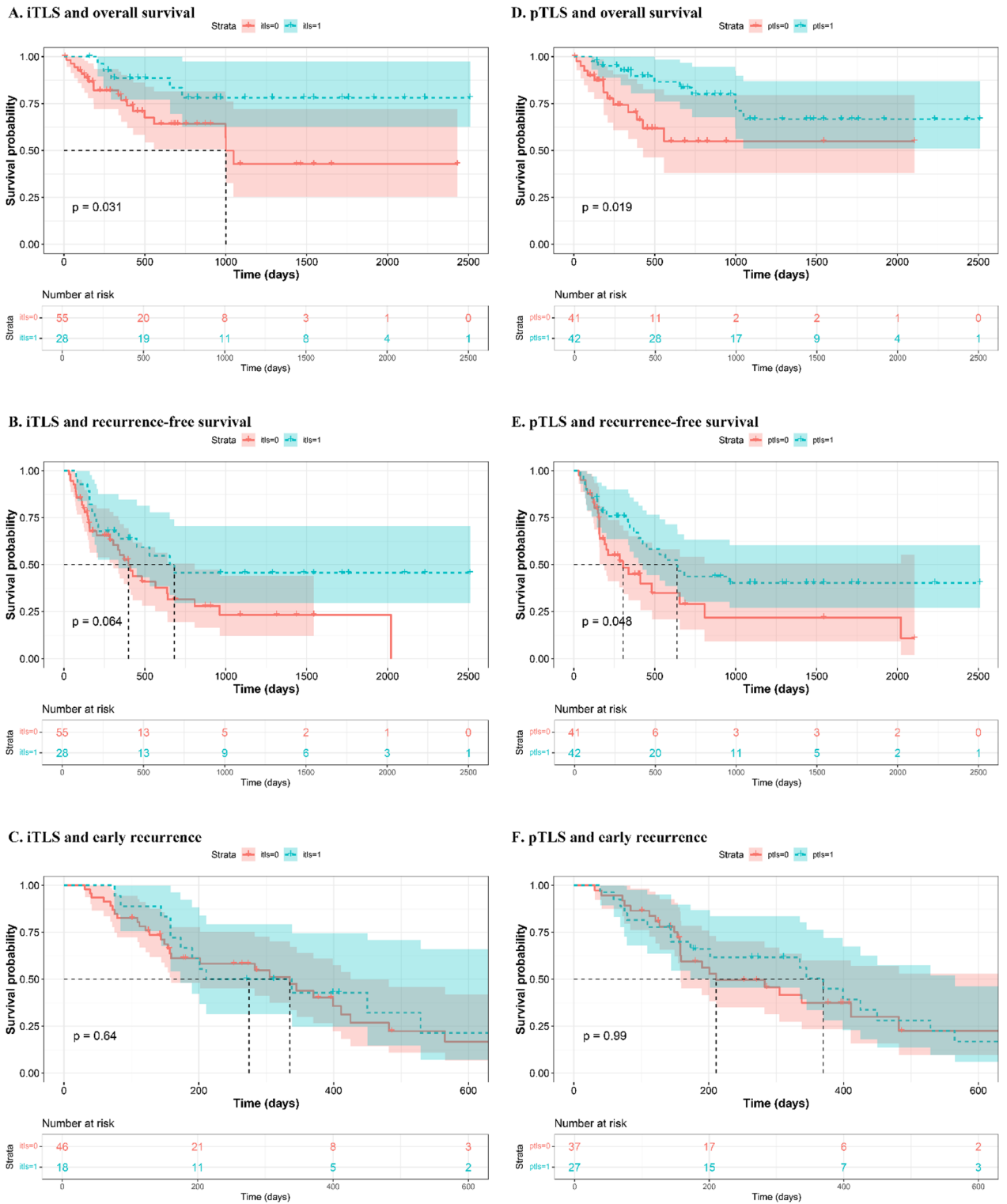


Fig. 5. The impact of intra-tumor tertiary lymphoid structures (iTLS) and peritumor tertiary lymphoid structures (pTLS) on overall survival (OS), recurrence-free survival (RFS), and early recurrence of patients in the Whole cohort based on Kaplan Meier survival curve. (A) iTLS was associated with better OS; (B) iTLS was not associated with RFS; (C) iTLS not associated with early recurrence; (D) pTLS was associated with better OS; (E) pTLS was not associated with RFS; (F) pTLS not associated with early recurrence.

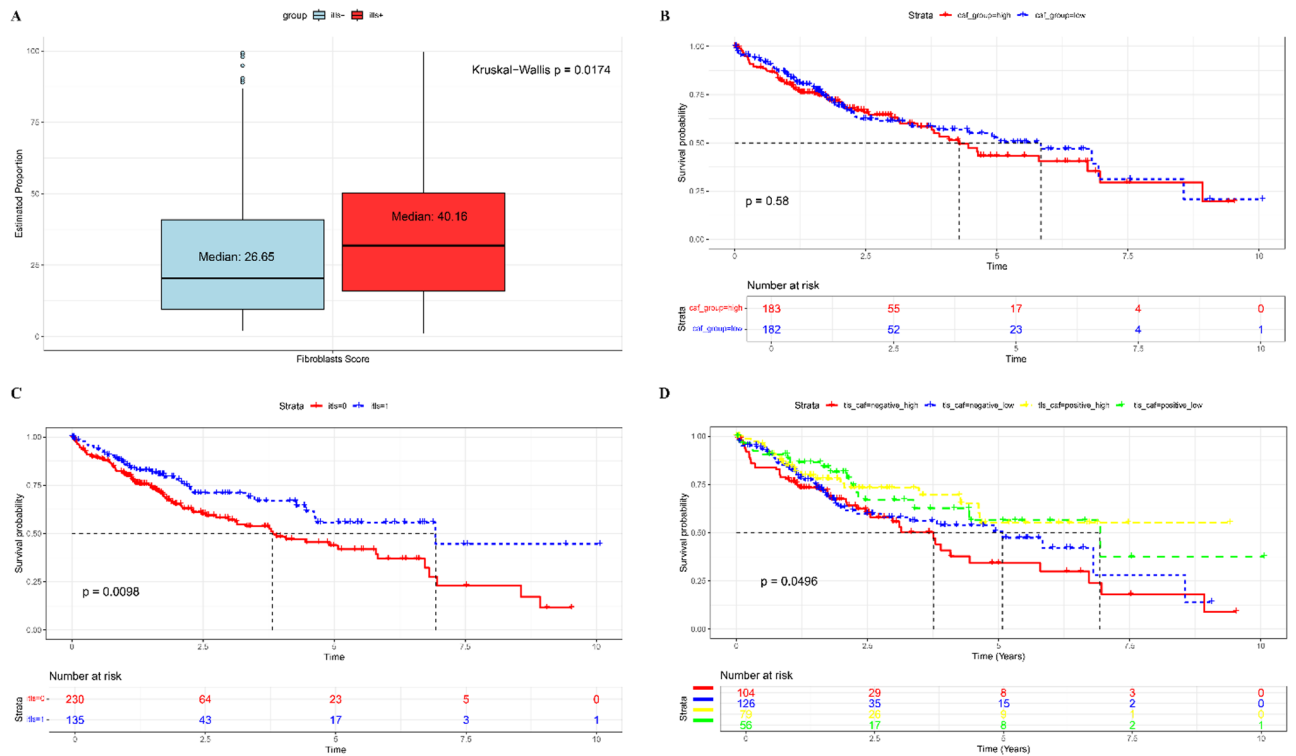


Fig. 6. The relationship between iTLS and cancer-related fibroblasts (CAF) scores with OS in TCGA cohort. **(A)** The difference between iTLS+ and iTLS- group; **(B)** Kaplan Meier curve based on CAF scores; **(C)** Kaplan Meier curve based on TLS status; **(D)** Kaplan Meier curve based on iTLS status and CAF scores.

Response to immunotherapy in high and low risk groups

We explored the differences in the response to immunotherapy between the high and low risk groups of the prognostic model using TIDE algorithm. In the TCGA, ICGC, CLCA sets, TIDE scores were higher in the high-risk group which means worse response to immunotherapy (Fig. 11A, D, and J). While the result in the GSE14520 set was opposite (Fig. 11G). Similarly, the percentages of patients' response to immunotherapy were significantly higher in the low-risk group in TCGA and ICGC sets (Fig. 11C, F), while the result was opposite in the GSE14520 set (Fig. 11I).

In the four datasets, this study performed univariate and multivariate Cox regression analysis on the risk score combined with clinical information. The results showed that risk score was significant for the prognosis of patients in all datasets (Fig. 12A-D). The results of multivariate Cox regression analysis showed the same conclusion except for the GSE14520 dataset (Fig. 12A-D). This shows that the prognostic model risk score constructed in this study can be used as an independent prognostic factor.

Immunohistochemistry of target gene

In the HPA database, we obtained the expression profiles of KLF2, CHORDC1, and YTHDF2 proteins in normal liver tissue and HCC tissue. The results indicated that KLF2 is expressed at low levels in hepatocytes and at moderate levels in HCC cells. CHORDC1 is also expressed at low levels in hepatocytes and at moderate levels in HCC cells. In contrast, YTHDF2 is expressed at moderate levels in hepatocytes and at low levels in HCC cells (Figure S5).

Discussion

This research sought to examine the predictive significance of the iTLS and pTLS in the prognosis of HCC patients with PVT following curative resection. The findings revealed that both iTLS + and pTLS + were correlated with improved OS across, yet they did not demonstrate any association with RFS or early recurrence. Because of the relationship we found between TLS and peri-tumoral fibrotic thickness, which is related to CAF³¹, we constructed a reliable prognostic assessment model based on TLS and CAF-related genes in HCC patients, which is important for achieving personalized treatment and improving patient survival.

The precise mechanism underlying the correlation between TLS and a favorable prognosis in HCC remains somewhat enigmatic. One hypothesis posits that tumor-associated TLS could stimulate tumor-infiltrating lymphocytes, thereby fostering robust antitumor immune responses. Enhanced levels of CD3+, CD8+, and CD20 + B cells were discerned in iTLS + instances, correlating with improved prognoses not only in HCC but also in various other solid tumors^{23,32,33}. Conversely, lower levels of intratumoral CD68 + macrophages were noted in TLS + cases, which have been linked to poorer prognoses in HCC^{23,33}. Moreover, TLS + cases exhibited diminished presence of immunosuppressive elements such as Foxp3 + Treg cells, PD1+, TIM3+, and LAG3 +

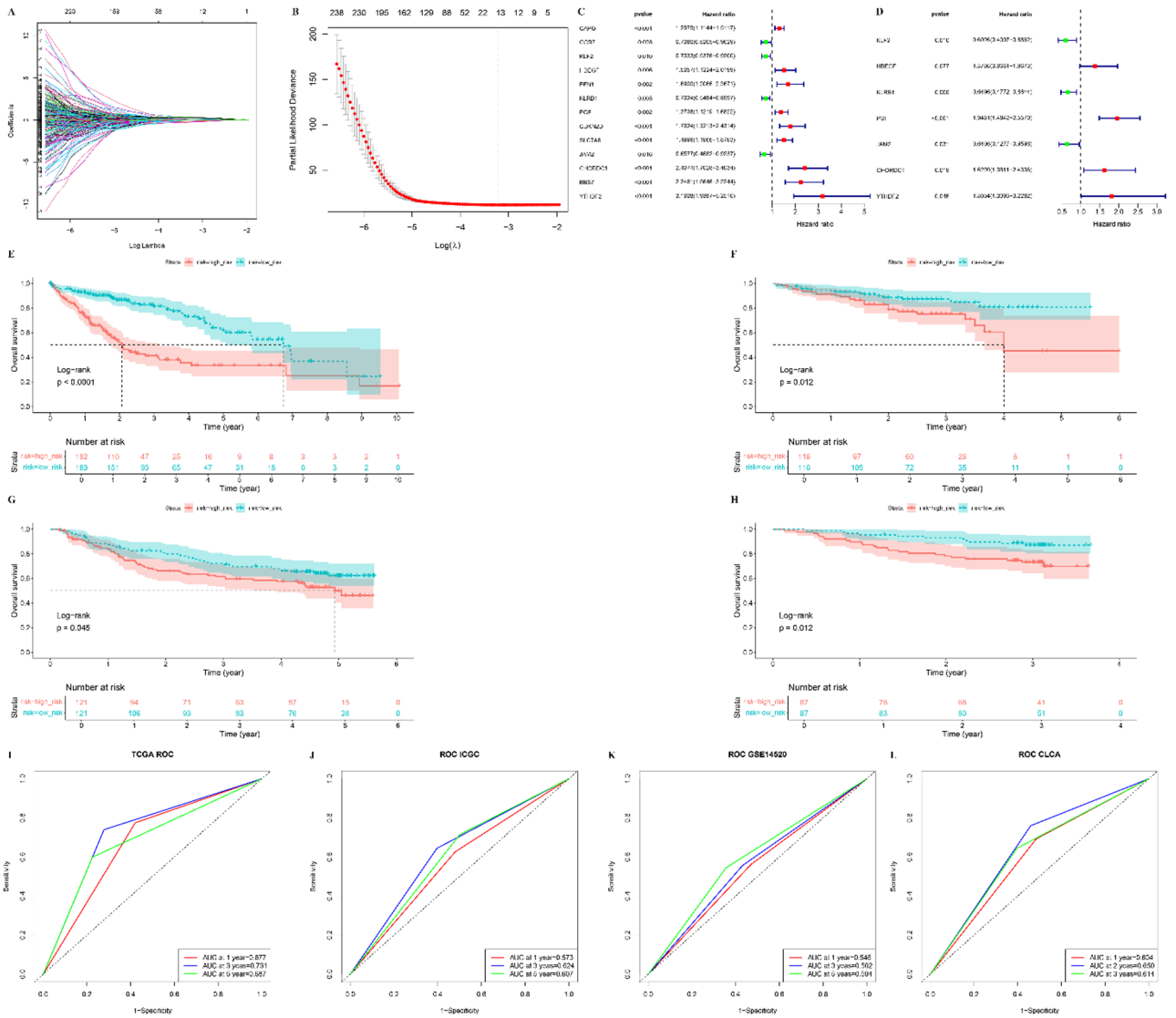


Fig. 7. Construction and validation of a prognostic model for hepatocellular carcinoma (HCC). **(A)** Coefficient profiles of genes derived from the LASSO Cox regression analysis. **(B)** Selection of the optimal penalty parameter (λ) for the LASSO model. **(C)** Forest plot of univariate Cox regression analysis for 13 candidate genes. **(D)** Forest plot of multivariate Cox regression analysis identifying 7 independent prognostic genes. **(E–H)** Kaplan-Meier survival curves comparing high-risk and low-risk groups in the TCGA, ICGC, GSE14520, and CLCA datasets, respectively (log-rank test). **(I–K)** Time-dependent receiver operating characteristic (ROC) curves assessing the predictive accuracy of the risk model at 1, 3, and 5 years in the TCGA, ICGC, and GSE14520 datasets. **(L)** Time-dependent ROC curves assessing the predictive accuracy of the risk model at 1, 2, and 3 years in the CLCA dataset.

cells, which may play roles in fostering host immune tolerance, facilitating cancer cells in evading antitumor immunity, and propelling tumor progression^{34–36}.

Concerning iTLS, its presence has been linked to improved RFS and early RFS^{23,24} while no association has been established with OS and late RFS^{23,24,37}. In our current investigation, we discovered that iTLS correlated with enhanced OS but not RFS and early recurrence in HCC patients with PVTT. Given that previous studies indicate approximately 25% of patients with BCLC B or C HCC, it can be inferred that iTLS + may exert divergent effects on the survival outcomes of patients with early and advanced HCC stages. Regarding pTLS, the relationship between heightened pTLS density and HCC patient survival has yielded inconsistent findings across prior studies³⁸. Finkin et al. observed that the presence of TLSs in non-tumoral liver tissue correlated with an elevated risk of late recurrence and a tendency toward diminished OS following surgical resection of HCC. Conversely, Zhang et al. demonstrated that pTLS + was associated with poorer OS and RFS outcomes compared to pTLS-³⁷. However, two other studies indicated that pTLS + was linked to enhanced OS and RFS. In our current investigation, we noted that pTLS + was associated with improved OS and exhibited a trend toward better RFS^{17,39}. Several factors may contribute to these disparate results. Firstly, variations in the definition and

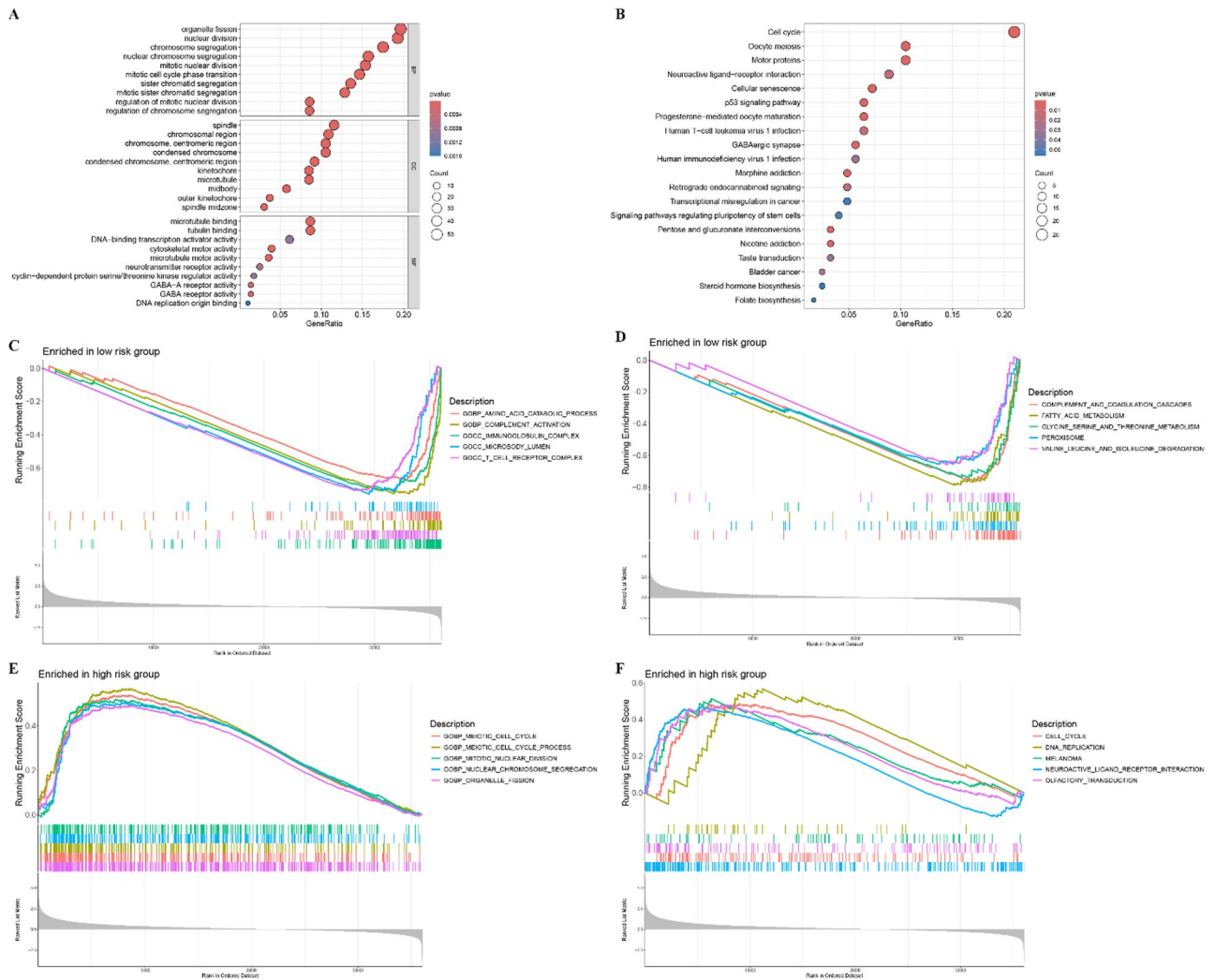


Fig. 8. Function annotation for differentially expressed genes (DEGs) related to risk score. **(A)** Functional annotation for DEGs using GO enrichment analysis. The size of the plots represented the number of genes enriched. The pathways were grouped by cellular component (CC), molecular function (MF) and biological process (BP). **(B)** Functional annotation for DEGs using KEGG enrichment analysis. The size of the plots represented the number of genes enriched. **(C, D)** Gene sets enrichment analysis (GSEA) in low-risk score group by GO and KEGG. **(E, F)** Gene sets enrichment analysis (GSEA) in high-risk score group by GO and KEGG.

methodology for delineating peritumoral tissue area among studies may lead to differing outcomes^{17,24,37,39}. We opted for a peritumoral 5 mm radius and utilized software to accurately calculate the peritumoral tissue area. Secondly, discrepancies in cutoff values for stratifying patients into distinct groups were evident. Lastly, tumor characteristics and clinical features varied across studies. Therefore, exploring the predictive role of TLS in HCC stratified by different tumor stages is imperative. This study serves as a valuable reference for understanding the role of TLS in hepatocellular carcinoma complicated by PVTT.

Additionally, the results indicated that iTLS + and high pTLS density were associated with improved OS, but not with RFS or early recurrence. Early recurrence in patients with hepatocellular carcinoma combined with portal vein tumor thrombus is associated with the type of portal vein tumor thrombus and is unrelated to the TLS status. This may be due to the low proportion of mature TLS in our sample. Early recurrence of liver cancer is related to the residual cancer cells⁴⁰, and mature TLS contain more advanced immune cells compared to immature TLS, thereby playing a more effective role in anti-tumor activity and inhibiting the growth of residual tumor cells^{41,42}. Patients with immature TLS, compared to those without TLS, have an immune environment in the liver with a higher number of immune cells, which can better exert anti-tumor effects and extend patient survival time^{41,42}. What is more, the timing and nature of immune responses is another factor related to this phenomenon.

CAF can secrete chemokines such as CXCL13, thereby promoting the formation of TLS⁴³. Since the presence of TLS is associated with better prognosis in cancer patients⁴², it logically follows that CAF might be linked to improved patient outcomes. However, existing studies indicate that CAF typically has immunosuppressive

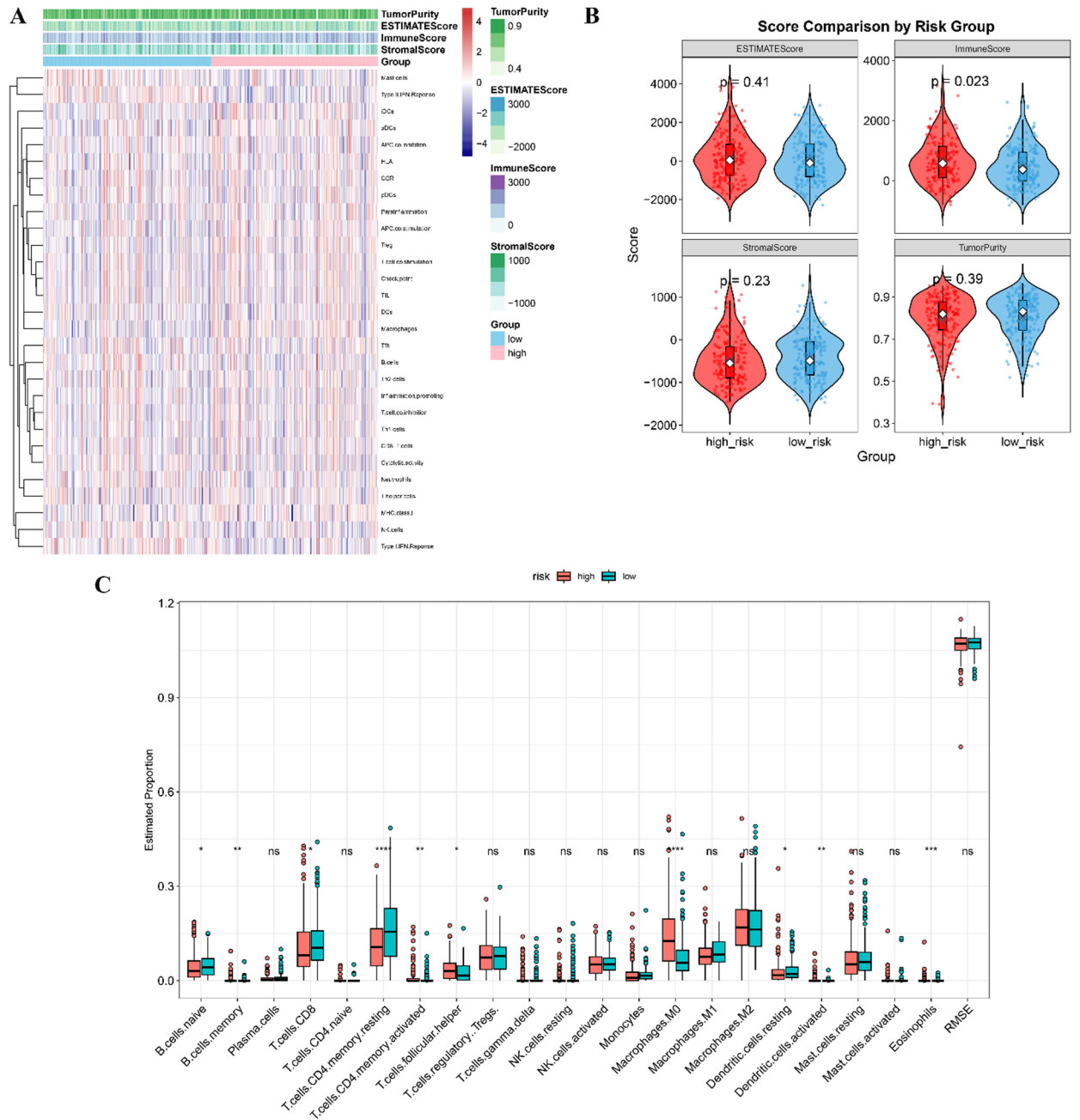


Fig. 9. Immune components between high and low risk groups. **(A).** Enrichment difference heat map of immune components and immune cells analyzed by ssGSEA method between high and low risk groups. **(B).** The immune score, ESTIMATE score, stromal score and tumor purity in the high and low risk groups. **(C).** CIBERSORT visualized the infiltration difference of immune cells between high and low risk groups, statistical significance was defined as $p < 0.05$. Significance levels are indicated as follows: *, $p < 0.05$, **, $p < 0.01$, ***, $p < 0.001$, and ****, $p < 0.0001$; ns, not significant..

effects and promotes tumor growth, leading to shorter survival times for patients⁴⁴. This apparent contradiction suggests that there may be unexplored interactions between CAF and TLS that jointly influence cancer patient prognosis⁴⁵. Recently, advanced single-cell technologies have revealed that specific CAF subtypes can exhibit functions conducive to anti-tumor immunity^{31,46}. The net effect of CAFs is likely determined by the balance between immunosuppressive and immune-supportive subtypes within the tumor microenvironment.

From previous literature, we identified TLS-related genes and CAF-related genes^{26,27}, and then performed correlation analysis to extract genes that are strongly correlated with these TLS and CAF-related genes as candidate genes. Based on these candidate genes, we constructed a prognostic model. Our model demonstrated good predictive ability for patient outcomes across four datasets. Moreover, this risk model was shown to be an

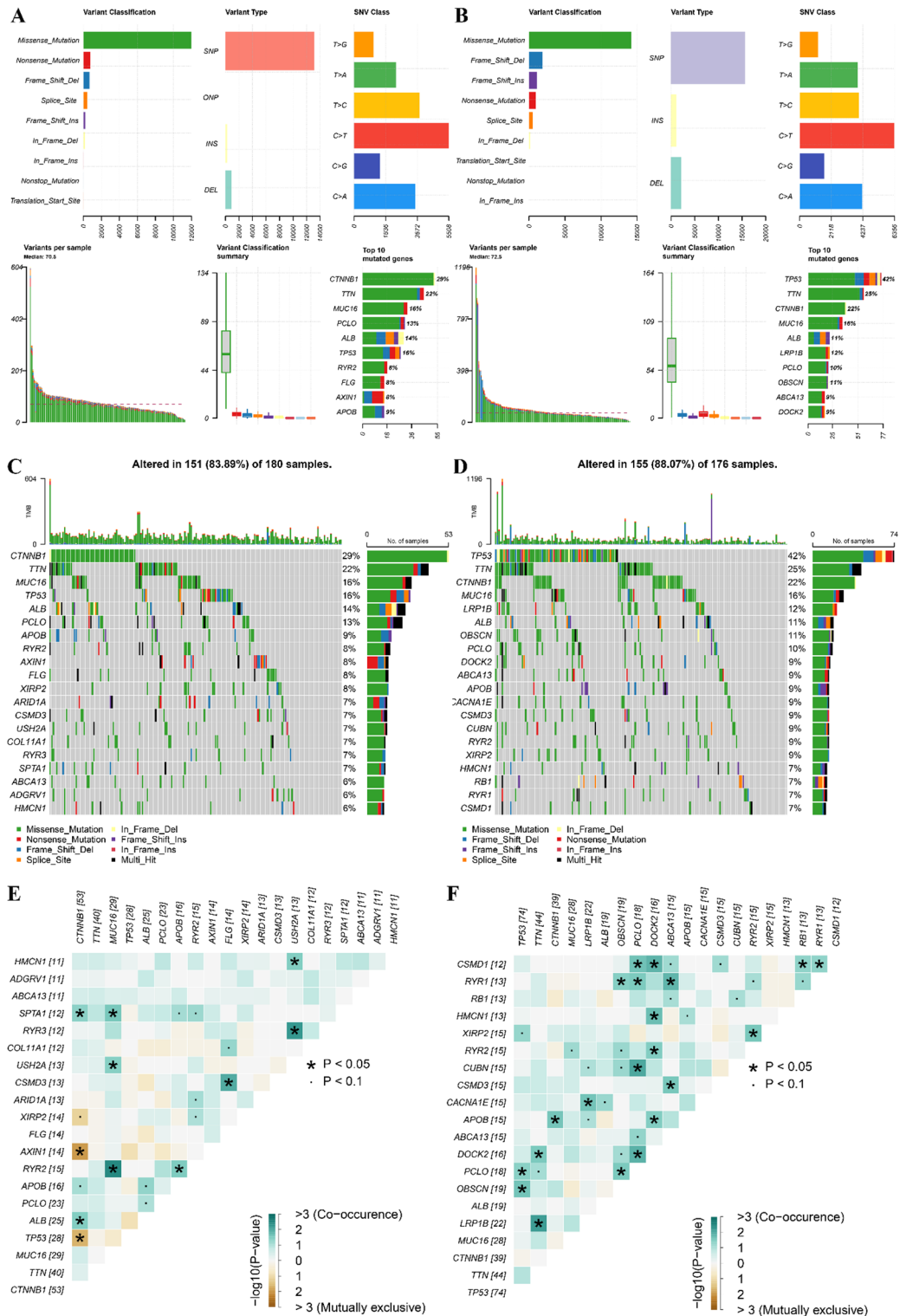


Fig. 10. Analysis of genomic mutation frequency in high and low risk groups. **(A, B)** Statistics of high-frequency mutation genes, mutation sites, and mutation types in the low-risk group and high-risk group. **(C, D)** The waterfall diagram of the mutation frequency top20 gene in the low-risk group and high-risk group. **(E, F)** Co-mutation and mutually exclusive mutation map of top20 gene in the whole group, low-risk group, and high-risk group.

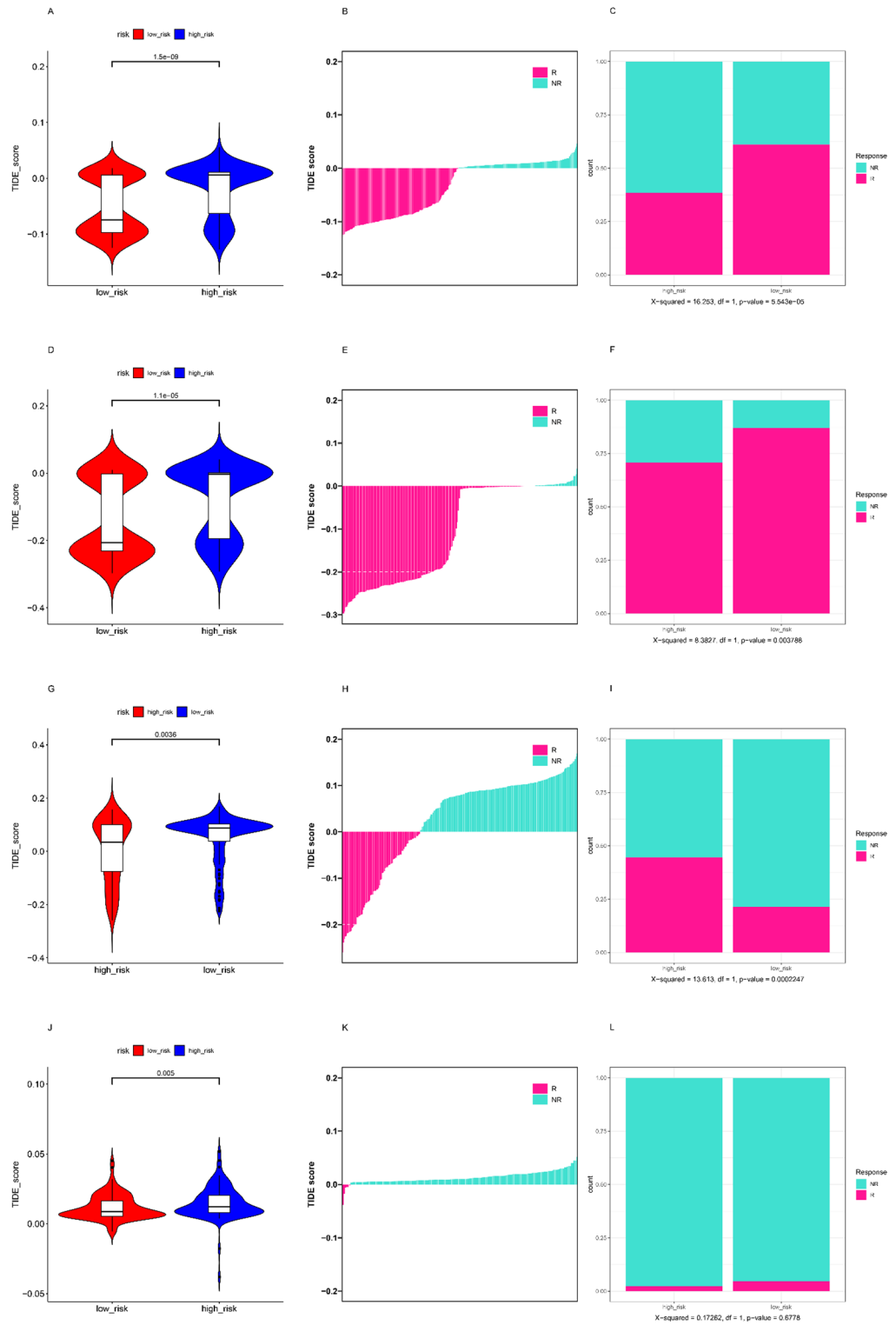


Fig. 11. Immunotherapy Response Assessment Using the TIDE Algorithm. (A–C). Comparison of the median TIDE score between high-risk and low-risk groups, individual TIDE scores for each sample, and the proportion of patients responding to immunotherapy in the TCGA cohort. (D–F). Same comparisons as in A–C, repeated in the ICGC cohort. (G–I). Further analysis of the GSE14520 cohort, comparing the median TIDE score between high-risk and low-risk groups, individual sample scores, and immunotherapy response rates. (J–L). Additional comparisons within the CLCA cohort, showing the median TIDE scores for high-risk vs. low-risk groups, individual sample scores, and patient response to immunotherapy.

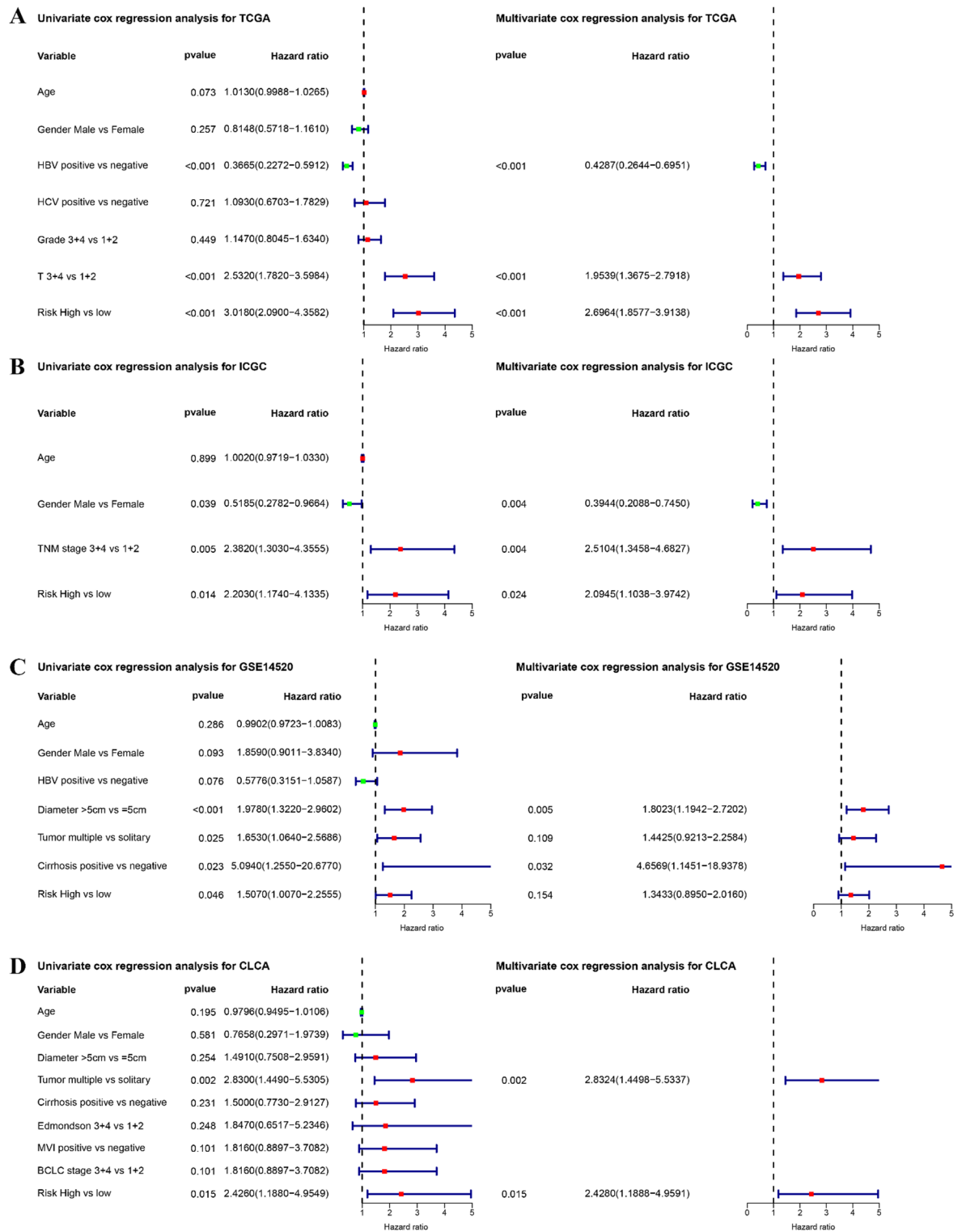


Fig. 12. Univariate and multivariate Cox regression analysis in the four datasets. (A) Univariate and multivariate Cox regression analysis in TCGA dataset, (B) Univariate and multivariate Cox regression analysis in ICGC dataset, (C) Univariate and multivariate Cox regression analysis in GSE14520 dataset, and (D) Univariate and multivariate Cox regression analysis in CLCA dataset.

independent risk factor for HCC patients in three datasets, indicating that the prognostic model we developed could serve as an independent predictive factor.

Risk models for HCC were constructed based on KLF2, HBEGF, KLRB1, PGF, JAM2, CHORDC1, and YTHDF2 genes using one-way cox analysis and LASSO regression algorithms. It was reported that KLF2 can

inhibit TGF- β -mediated cancer cell motility, thus affecting HCC development⁴⁷. Additionally, KLF2 could be silenced by Long non-coding RNAs, thus affecting HCC progression^{48–50}. Hence, KLF2 was reported as a promising marker in HCC and could be used as a prognostic marker associated with fibrosis and immune infiltration for advanced HCC⁵¹. It was reported that HBEGF played a role in the development or progression of human HCC in an autocrine and/or a juxtacrine manners⁵² and could be regulated by TMPRSS4 to promote HCC proliferation, invasion, and angiogenesis⁵³. KLRB1 was the gene encoding CD161, which has been shown to inhibit the cytotoxicity of NK cells. Thus, KLRB1 downregulates the inhibitory molecule CD161 and enhances the ability of NK cells to kill infected or transformed cells^{54,55}. It was reported that targeting PGF significantly decreases tumor burden by inhibiting neovascularization, decreasing hepatic macrophage recruitment, and by normalizing the remaining blood vessels, thereby decreasing hypoxia and reducing the premetastatic potential of HCC⁵⁶. JAM2 is a potential marker for a subfraction of hematopoietic stem cells with an extensive lymphopoietic capacity, mainly in T lymphopoiesis⁵⁷. However, the study of JAM2 in hepatocellular carcinoma is less, and it may lead to a good prognosis. The study of CHORDC1 in hepatocellular carcinoma is less, but and it may lead to a worse prognosis⁵⁸. It was reported that O-GlcNAcylation of YTHDF2 promotes hepatocellular carcinoma progression in an N6-methyladenosine-dependent manner^{59,60}.

We also explored the differences in biological processes, molecular function, and immune microenvironment between high-risk and low-risk groups in the prognostic model. In terms of biological processes, the differences were primarily concentrated in tumor proliferation. In the high-risk group, the functions enriched among highly expressed genes were related to tumor proliferation, such as organelle fission, nuclear division, and chromosome segregation. This suggests that tumor cells in the high-risk group are more actively proliferating compared to those in the low-risk group, which is one reason for the poorer prognosis in the high-risk group. Additionally, we found that the functions of highly expressed genes in the low-risk group were enriched in T cells and immunoglobulins. Furthermore, the CIBERSORT results showed that the low-risk group had higher quantities of immune cells, including B cells, T cells, and dendritic cells, compared to the high-risk group. These findings indicate that the low-risk group has a higher number of immune cells in the tumor microenvironment, thereby improving the prognosis for this group of patients. Moreover, we observed that the TIDE scores were higher in the high-risk group across three datasets, indicating that patients in the high-risk group were less responsive to immunotherapy. This suggests that our model could potentially be used as a screening tool to determine whether HCC patients would benefit from immunotherapy. Additionally, we observed that the low-risk group exhibits fewer co-mutations but more mutually exclusive mutations. This suggests that mutations in the low-risk group tend to be mutually exclusive, leading to distinct carcinogenic pathways. This implies that the low-risk group may have more defined and independent molecular mechanisms, with tumor formation relying on specific key mutational pathways. Conversely, in the high-risk group, the presence of more co-mutations and fewer mutually exclusive mutations indicates a more complex mutation landscape involving multiple concurrent mutations. This complexity may allow the tumor to evolve through several mutational pathways, thereby increasing its aggressiveness and complicating treatment. Overall, these findings highlight the differing mutational patterns and potential biological behaviors between the risk groups in HCC, potentially impacting therapeutic responses and prognosis.

Several limitations warrant attention. Primarily, this study is a single-center retrospective analysis, characterized by a relatively modest sample size, thereby inevitably harboring inherent biases. Furthermore, the findings of this study necessitate validation through larger-scale investigations. Secondly, the adequacy of a single slice to comprehensively depict the actual status of TLS within the tumor and peritumoral tissue raises legitimate concerns. Thus, the development of more judicious methodologies for assessing TLS is imperative. In addition, the model feature genes mined in this study need to be further verified by cell or tissue experiments to further verify their actual role in cancer progression or patient prognosis. Despite these limitations, our study stands as the inaugural exploration showcasing the prognostic significance of iTLS and pTLS for HCC patients with PVTT. What is more, the generalizability of the constructed model may be influenced by the patient characteristics and clinical backgrounds among the external validation cohorts. We included four cohorts from three regions: China, Japan, and the United States. Our model demonstrated good predictive performance across all four cohorts.

Conclusion

This study investigated the prognostic significance of intratumoral (iTLS) and peritumoral tertiary lymphoid structures (pTLS) in hepatocellular carcinoma (HCC) patients with portal vein tumor thrombus (PVTT) after curative resection. The results showed that iTLS+ and pTLS+ were associated with improved overall survival (OS), although no correlation was found with recurrence-free survival (RFS) or early recurrence. Based on the relationship between TLS and cancer-associated fibroblasts (CAF), a prognostic model incorporating TLS and CAF-related genes was developed, demonstrating robust predictive power for patient outcomes and serving as an independent prognostic factor. The mechanisms behind the favorable prognosis of TLS in HCC remain unclear but may involve enhanced antitumor immune responses, as suggested by elevated CD3+, CD8+, and CD20+ B cells in iTLS+ cases and reduced immunosuppressive cells. Moreover, the study explored the biological differences between high- and low-risk groups in the model, finding that tumor proliferation was more active in the high-risk group, while the low-risk group had greater immune cell infiltration. Despite limitations, including the single-center retrospective design and the need for further validation, this research is the first to highlight the prognostic relevance of iTLS and pTLS in HCC with PVTT, offering a new avenue for predicting patient outcomes and guiding personalized treatment.

Data availability

The datasets used and/or analysed during the current study available from the corresponding author on reasonable request.

Received: 8 February 2025; Accepted: 10 November 2025

Published online: 23 November 2025

References

- Sung, H. et al. Global cancer statistics 2020: GLOBOCAN estimates of incidence and mortality worldwide for 36 cancers in 185 countries. *CA Cancer J. Clin.* **71** (3), 209–249 (2021).
- Villanueva, A. Hepatocellular carcinoma. *N Engl. J. Med.* **380** (15), 1450–1462 (2019).
- Fornier, A., Reig, M. & Bruix, J. Hepatocellular carcinoma. *Lancet* **391** (10127), 1301–1314 (2018).
- EASL Clinical Practice Guidelines. Management of hepatocellular carcinoma. *J. Hepatol.* **69** (1), 182–236 (2018).
- Singal, A. G. et al. AASLD practice guidance on prevention, diagnosis, and treatment of hepatocellular carcinoma. *Hepatology* (2023).
- Hyun, M. H. et al. Hepatic resection compared to chemoembolization in intermediate- to advanced-stage hepatocellular carcinoma: A meta-analysis of high-quality studies. *Hepatology* **68** (3), 977–993 (2018).
- Choi, K. K. et al. Portal venous invasion: the single most independent risk factor for immediate postoperative recurrence of hepatocellular carcinoma. *J. Gastroenterol. Hepatol.* **26** (11), 1646–1651 (2011).
- Chen, Z. H. et al. Actual long-term survival in hepatocellular carcinoma patients with microvascular invasion: a multicenter study from China. *Hepatol. Int.* **15** (3), 642–650 (2021).
- Shinkawa, H. et al. Nomograms predicting extra- and early intrahepatic recurrence after hepatic resection of hepatocellular carcinoma. *Surgery* **169** (4), 922–928 (2021).
- Chen, Z. H. et al. Actual long-term survival in HCC patients with portal vein tumor thrombus after liver resection: a nationwide study. *Hepatol. Int.* **14** (5), 754–764 (2020).
- Orimo, T. et al. Hepatectomy is beneficial in select patients with multiple hepatocellular carcinomas. *Ann. Surg. Oncol.* **29** (13), 8436–8445 (2022).
- Kokudo, T. et al. Survival benefit of liver resection for hepatocellular carcinoma associated with portal vein invasion. *J. Hepatol.* **65** (5), 938–943 (2016).
- Yao, L. Q. et al. Clinical features of recurrence after hepatic resection for Early-Stage hepatocellular carcinoma and Long-Term survival outcomes of patients with recurrence: A Multi-institutional analysis. *Ann. Surg. Oncol.* (2022).
- Fridman, W. H., Zitvogel, L., Sautès-Fridman, C. & Kroemer, G. The immune contexture in cancer prognosis and treatment. *Nat. Rev. Clin. Oncol.* **14** (12), 717–734 (2017).
- Wang, X. et al. Spatial relationship of tertiary lymphoid structures and tumor-associated neutrophils in bladder cancer and prognostic potential for anti-PD-L1 immunotherapy. *Cancer Commun. (Lond)* (2023).
- Bruni, D., Angell, H. K. & Galon, J. The immune contexture and immunoscore in cancer prognosis and therapeutic efficacy. *Nat. Rev. Cancer.* **20** (11), 662–680 (2020).
- Wen, S. D. et al. Combination of tertiary lymphoid structure and Neutrophil-to-Lymphocyte ratio predicts survival in patients with hepatocellular carcinoma. *Front. Immunol.* ;**12**. (2022).
- Lee, M. et al. Presence of tertiary lymphoid structures determines the level of tumor-infiltrating lymphocytes in primary breast cancer and metastasis. *Mod. Pathol.* **32** (1), 70–80 (2019).
- Siliņa, K. et al. Germinal centers determine the prognostic relevance of tertiary lymphoid structures and are impaired by corticosteroids in lung squamous cell carcinoma. *Cancer Res.* **78** (5), 1308–1320 (2018).
- Posch, F. et al. Maturation of tertiary lymphoid structures and recurrence of stage II and III colorectal cancer. *Oncoimmunology* **7** (2), e1378844 (2018).
- Zou, X. et al. Characterization of intratumoral tertiary lymphoid structures in pancreatic ductal adenocarcinoma: cellular properties and prognostic significance. *J. Immunother. Cancer* ;**11**(6). (2023).
- Jia, W. L. et al. Protective effect of tertiary lymphoid structures against hepatocellular carcinoma: new findings from a genetic perspective. *Front. Immunol.* ;**13**. (2022).
- Li, H. et al. Existence of intratumoral tertiary lymphoid structures is associated with immune cells infiltration and predicts better prognosis in early-stage hepatocellular carcinoma. *Aging-U.S.* **12** (4), 3451–3472 (2020).
- Calderaro, J. et al. Intra-tumoral tertiary lymphoid structures are associated with a low risk of early recurrence of hepatocellular carcinoma. *J. Hepatol.* **70** (1), 58–65 (2019).
- Chen, L. et al. Deep whole-genome analysis of 494 hepatocellular carcinomas. *Nature* **627** (8004), 586–593 (2024).
- Sautès-Fridman, C., Petitprez, F., Calderaro, J. & Fridman, W. H. Tertiary lymphoid structures in the era of cancer immunotherapy. *Nat. Rev. Cancer.* **19** (6), 307–325 (2019).
- Yuan, Q. et al. CAFrgDB: a database for cancer-associated fibroblasts related genes and their functions in cancer. *Cancer Gene Ther.* **30** (6), 917–925 (2023).
- Kanehisa, M. & Goto, S. KEGG: Kyoto encyclopedia of genes and genomes. *Nucleic Acids Res.* **28** (1), 27–30 (2000).
- Kanehisa, M. Toward Understanding the origin and evolution of cellular organisms. *Protein Sci.* **28** (11), 1947–1951 (2019).
- Kanehisa, M., Furumichi, M., Sato, Y., Kawashima, M. & Ishiguro-Watanabe, M. KEGG for taxonomy-based analysis of pathways and genomes. *Nucleic Acids Res.* **51** (D1), D587–d92 (2023).
- Cheng, Y. et al. Stromal architecture and fibroblast subpopulations with opposing effects on outcomes in hepatocellular carcinoma. *Cell. Discov.* **11** (1), 1 (2025).
- Goc, J. et al. Dendritic cells in tumor-associated tertiary lymphoid structures signal a Th1 cytotoxic immune contexture and license the positive prognostic value of infiltrating CD8 + T cells. *Cancer Res.* **74** (3), 705–715 (2014).
- Zhang, Z. et al. Landscape of infiltrating B cells and their clinical significance in human hepatocellular carcinoma. *Oncoimmunology* **8** (4), e1571388 (2019).
- Shields, J. D., Kourtis, I. C., Tomei, A. A., Roberts, J. M. & Swartz, M. A. Induction of lymphoidlike stroma and immune escape by tumors that express the chemokine CCL21. *Science* **328** (5979), 749–752 (2010).
- Gobert, M. et al. Regulatory T cells recruited through CCL22/CCR4 are selectively activated in lymphoid infiltrates surrounding primary breast tumors and lead to an adverse clinical outcome. *Cancer Res.* **69** (5), 2000–2009 (2009).
- Narayanan, S. et al. Tumor infiltrating lymphocytes and macrophages improve survival in microsatellite unstable colorectal cancer. *Sci. Rep.* **9** (1), 13455 (2019).
- Zhang, T. et al. Peritumor tertiary lymphoid structures are associated with infiltrating neutrophils and inferior prognosis in hepatocellular carcinoma. *Cancer Med.* **12** (3), 3068–3078 (2023).
- Finkin, S. et al. Ectopic lymphoid structures function as microniches for tumor progenitor cells in hepatocellular carcinoma. *Nat. Immunol.* **16** (12), 1235–1244 (2015).
- Li, H. et al. Peritumoral tertiary lymphoid structures correlate with protective immunity and improved prognosis in patients with hepatocellular carcinoma. *Front. Immunol.* **12**, 648812 (2021).

40. Nevola, R. et al. Predictors of early and late hepatocellular carcinoma recurrence. *World J. Gastroenterol.* **29** (8), 1243–1260 (2023).
41. Radandish, M. et al. In-depth insight into tumor-infiltrating stromal cells linked to tertiary lymphoid structures and their prospective function in cancer immunotherapy. *Exp. Hematol. Oncol.* **14** (1), 105 (2025).
42. Schumacher, T. N. & Thommen, D. S. Tertiary lymphoid structures in cancer. *Science* **375** (6576), eabf9419 (2022).
43. O'Connor, R. A., Martinez, B. R., Koppensteiner, L., Mathieson, L. & Akram, A. R. Cancer-associated fibroblasts drive CXCL13 production in activated T cells via TGF- β . *Front. Immunol.* **14**, 1221532 (2023).
44. Farhood, B., Najafi, M. & Mortezaee, K. Cancer-associated fibroblasts: Secretions, interactions, and therapy. *J. Cell. Biochem.* **120** (3), 2791–2800 (2019).
45. Mao, X. et al. Crosstalk between cancer-associated fibroblasts and immune cells in the tumor microenvironment: new findings and future perspectives. *Mol. Cancer.* **20** (1), 131 (2021).
46. Rodriguez, A. B. et al. Immune mechanisms orchestrate tertiary lymphoid structures in tumors via cancer-associated fibroblasts. *Cell. Rep.* **36** (3), 109422 (2021).
47. Li, Y. et al. KLF2 inhibits TGF- β -mediated cancer cell motility in hepatocellular carcinoma. *Acta Biochim. Biophys. Sin (Shanghai).* **52** (5), 485–494 (2020).
48. Huang, M. D. et al. Long non-coding RNA TUG1 is up-regulated in hepatocellular carcinoma and promotes cell growth and apoptosis by epigenetically silencing of KLF2. *Mol. Cancer.* **14**, 165 (2015).
49. Huang, M. D. et al. Long non-coding RNA ANRIL is upregulated in hepatocellular carcinoma and regulates cell apoptosis by epigenetic silencing of KLF2. *J. Hematol. Oncol.* **8**, 50 (2015).
50. Jin, L., He, Y., Tang, S. & Huang, S. LncRNA GHET1 predicts poor prognosis in hepatocellular carcinoma and promotes cell proliferation by silencing KLF2. *J. Cell. Physiol.* **233** (6), 4726–4734 (2018).
51. Chen, X. Q., Ma, J., Xu, D. & Xiang, Z. L. Comprehensive analysis of KLF2 as a prognostic biomarker associated with fibrosis and immune infiltration in advanced hepatocellular carcinoma. *BMC Bioinform.* **24** (1), 270 (2023).
52. Inui, Y. et al. Expression of heparin-binding epidermal growth factor in human hepatocellular carcinoma. *Gastroenterology* **107** (6), 1799–1804 (1994).
53. Dong, Z. R. et al. TMPRSS4 drives angiogenesis in hepatocellular carcinoma by promoting HB-EGF expression and proteolytic cleavage. *Hepatology* **72** (3), 923–939 (2020).
54. Aldemir, H. et al. Cutting edge: lectin-like transcript 1 is a ligand for the CD161 receptor. *J. Immunol.* **175** (12), 7791–7795 (2005).
55. Fang, S. & Zhou, Y. Deciphering the role of KLRB1: a novel prognostic indicator in hepatocellular carcinoma. *BMC Gastroenterol.* **24** (1), 210 (2024).
56. Heindryckx, F. et al. The placental growth factor as a target against hepatocellular carcinoma in a diethylnitrosamine-induced mouse model. *J. Hepatol.* **58** (2), 319–328 (2013).
57. Radulovic, V. et al. Junctional adhesion molecule 2 represents a subset of hematopoietic stem cells with enhanced potential for T lymphopoiesis. *Cell. Rep.* **27** (10), 2826–36e5 (2019).
58. Hu, B., Qu, C., Qi, W. J., Liu, C. H. & Xiu, D. R. Development and verification of the glycolysis-associated and immune-related prognosis signature for hepatocellular carcinoma. *Front. Genet.* **13**, 955673 (2022).
59. Hou, J. et al. YTHDF2 reduction fuels inflammation and vascular abnormalization in hepatocellular carcinoma. *Mol. Cancer.* **18** (1), 163 (2019).
60. Yang, Y. et al. O-GlcNAcylation of YTHDF2 promotes HBV-related hepatocellular carcinoma progression in an N(6)-methyladenosine-dependent manner. *Signal. Transduct. Target. Ther.* **8** (1), 63 (2023).

Author contributions

L.H. and C.C. designed this project. L.H., Y.X. and Z.L. participated in data acquisition. L.H. and Z.L. performed data analyses, interpretation. G.L. and J.T. visualized all the results. L.H. drafted the manuscript. B.Z., C.D. and N.J. revised the manuscript. All the authors reviewed the manuscript and approved its final version.

Funding

This work was supported by the National Natural Science Foundation of China (No. 82203310), Technological Innovation and Application Project of Chongqing (No. CSTB2024TIAD-LUX0003), and Natural Science Foundation of Chongqing (CSTB2022NSCQ-MSX0063).

Declarations

Competing interests

The authors declare no competing interests.

Ethics approval and consent to participate

The study was performed according to Strengthening the Reporting of Cohort Studies in Surgery (STROCSS) guidelines and after Institutional Review Board ‘The First Affiliated Hospital of Chongqing Medical University’ approval for data collection (protocol number K2023-440), all institutions obtained their respective approvals according to their local center requirements.

Consent for publication

All authors consented for publication.

Additional information

Supplementary Information The online version contains supplementary material available at <https://doi.org/10.1038/s41598-025-28296-9>.

Correspondence and requests for materials should be addressed to G.L., J.T. or B.Z.

Reprints and permissions information is available at www.nature.com/reprints.

Publisher’s note Springer Nature remains neutral with regard to jurisdictional claims in published maps and institutional affiliations.

Open Access This article is licensed under a Creative Commons Attribution-NonCommercial-NoDerivatives 4.0 International License, which permits any non-commercial use, sharing, distribution and reproduction in any medium or format, as long as you give appropriate credit to the original author(s) and the source, provide a link to the Creative Commons licence, and indicate if you modified the licensed material. You do not have permission under this licence to share adapted material derived from this article or parts of it. The images or other third party material in this article are included in the article's Creative Commons licence, unless indicated otherwise in a credit line to the material. If material is not included in the article's Creative Commons licence and your intended use is not permitted by statutory regulation or exceeds the permitted use, you will need to obtain permission directly from the copyright holder. To view a copy of this licence, visit <http://creativecommons.org/licenses/by-nc-nd/4.0/>.

© The Author(s) 2025